Saeedian, Meysam; Gomis-Bellmunt, Oriol; Pouresmaeil, Edris

Multiobjective Laguerre Functions−Based Discrete−Time Model Predictive Control: A Fast Inner−Loop Controller for Grid−Forming Converters

Published in:
Electric Power Systems Research

DOI:
10.1016/j.epsr.2022.107976

Published: 01/01/2022

Document Version
Publisher's PDF, also known as Version of record

Please cite the original version:
Saeedian, M., Gomis-Bellmunt, O., & Pouresmaeil, E. (2022). Multiobjective Laguerre Functions−Based Discrete−Time Model Predictive Control: A Fast Inner−Loop Controller for Grid−Forming Converters. *Electric Power Systems Research*, *209*, 1-10. Article 107976. https://doi.org/10.1016/j.epsr.2022.107976

Electric Power Systems Research 209 (2022) 107976

Contents lists available at ScienceDirect

Electric Power Systems Research

journal homepage: www.elsevier.com/locate/epsr

Multiobjective Laguerre Functions – Based Discrete – Time Model Predictive Control: A Fast Inner – Loop Controller for Grid – Forming Converters

Meysam Saeedian [a], Oriol Gomis-Bellmunt [b], Edris Pouresmaeil [*,a]

[a] Department of Electrical Engineering and Automation, Aalto University, Espoo, Finland
[b] Centre d'Innovacio Tecnologica en Convertidors Estatics i Accionaments, Departament d'Enginyeria Electrica, Universitat Politecnica de Catalunya, Barcelona, Spain

ARTICLE INFO

Keywords:
Ac microgrid
Virtual synchronous generator
Model predictive control
Large prediction horizon
Overcurrent protection

ABSTRACT

In islanded ac microgrids, conventional primary control uses inner – loop cascaded linear controller and outer – loop droop to realize local voltage regulation and power sharing. However, it has a poor dynamic performance and fast rate of frequency change following disturbances. This paper addresses these issues by proposing a modified virtual synchronous generator (VSG) control. A Laguerre functions – based discrete – time model predictive control (LF – DMPC) with a multiobjective cost function is incorporated as the inner loop; yielding large prediction horizon, improved dynamic response, and inherent overcurrent protection in the case of faults. The swing – based and the reactive power droop controllers also form the outer loop aimed at inertia emulation and power sharing. The merits of proposed approach are verified by comparisons with conventional droop and VSG controls. Detailed model simulations are conducted on a 2 – converter ac microgrid in MATLAB/Simulink to show the efficacy of the proposed controller.

1. Introduction

The paradigm of grid – connected and islanded mode ac microgrids were introduced to enhance system stability and resiliency of wider integrated power electronic – based generators [1]. At the heart of microgrid is VSCs, operating as the interface between distributed energy resources and common ac bus. Generally, VSC controllers are categorized as grid – following and grid – forming. Thereof, the former one features current – stiff operation; i.e., the output voltage of VSC is controlled through a current regulator. Synchronization with the host microgrid is fulfilled by a phase – locked loop (PLL) connected to the PoI. High concentration of grid – following converters may yield various converter – grid instability phenomena [2,3]. In contrast, grid – forming converter is partly implied voltage – stiff operation; i.e., operation with near – constant converter voltage magnitude, and partly the emulation of a droop or swing equation (realizing synchronization with the host microgrid) [4]. This type is the crucial element for preserving the stability of microgrids dominated by converter – interfaced generation. Herein, the grid – forming converter is only discussed and the readers are referred to [5] about grid – following type.

1.1. Review of the Literature

A plethora of control mechanisms have been hitherto introduced for VSCs in grid – forming mode. Ref. [6] proposes a grid – forming VSC aimed at supporting frequency and voltage of microgrids. It comprises two main loops; in the external loop, a swing equation is adopted and the inner loop is realized by a sliding mode – based vector control which applies a constant switching frequency. An automatic tuning algorithm of cascaded linear controller using eigenvalue parametric sensitivities is introduced in [7]. This method ensures the stability and improved dynamic response of control systems with multiple cascaded loops. In [8], quantitative feedback theory is applied to regulate the parameters of a VSG operating in microgrid. Indeed, it provides a combination of the virtual rotor, virtual primary and secondary controllers to enhance the load – frequency characteristic in the microgrid. A frequency controller is presented in [9] for islanded microgrids composed of conventional SGs and power electronic – based generation. This approach first estimates the power imbalance during transients using an approximated linear model of the microgrid. The compensated power is then provided by a battery – type energy storage controlled via the state of charge algorithm. Ref. [10] proposes a VSG augmented with pole placement – based state feedback controller to suppress microgrid frequency

* Corresponding author.
E-mail address: edris.pouresmaeil@aalto.fi (E. Pouresmaeil).

https://doi.org/10.1016/j.epsr.2022.107976
Received 16 December 2021; Received in revised form 21 March 2022; Accepted 29 March 2022
Available online 13 April 2022

Abbreviations

ESS	Energy storage system
PoI	Point of interconnection
RoCoF	Rate of change of frequency
SG	Synchronous generator
SRF	Synchronous reference frame
SS – PWM	Symmetrical suboscillation pulse – width modulation
VSC	Voltage – source converter
VSG	Virtual synchronous generator

Variables

$\boldsymbol{i}_c$	Converter – side current
$\boldsymbol{i}_g$	Grid – side current
p_g, q_g	Converter output power
p_{load}	Load demand
$\boldsymbol{u}_c^\star$	Control signal
$\boldsymbol{u}_c$	Converter voltage
$\boldsymbol{u}_f$	Capacitor voltage
$\boldsymbol{u}_t$	PoI voltage
u_{dc}	dc – link voltage
$\lvert u \rvert$	Amplitude of capacitor voltage reference
ω_g	Grid angular frequency
ϑ_g	Phase angle

Parameters

C_f	Filter capacitor
D	Damping factor
f_{sw}	Switching frequency
$I_{c,max}$	Maximum allowable inductor current
J	Moment of inertia
k_{pi}, k_{ii}	Current controller gains
k_{pu}, k_{iu}	Voltage controller gains
L_{fc}	Converter – side filter inductance
L_{fg}	Grid – side filter inductance
L_{line}	Transmission line inductance
m_p, m_q	Droop coefficients
N	Number of terms used in Laguerre function expansion
N_c	Control horizon
N_p	Prediction horizon
$p_g^\star, q_g^\star$	Converter output power reference
r_i	Current feedforward gain
R_{fc}	Converter – side filter resistance
R_{fg}	Grid – side filter resistance
R_{line}	Transmission line resistance
u_{fN}	PoI voltage reference
ω_n	Grid nominal angular frequency
Z_{vi}	Virtual impedance
α	Scaling factor in Laguerre functions
$\boldsymbol{\eta}_c$	Parameter vector in Laguerre expansion
$\mathbf{L}_c$	Vector form of Laguerre functions

oscillations. Moreover, the improvement in dynamic response and robust operation is achieved by genetic algorithm optimized VSG parameters. The cascaded linear control of a grid – forming converter is superseded by a finite control set model predictive control (FCS – MPC) in [11]. Hence, it yields a simpler control structure and faster transient performance compared to the cascaded linear control. In contrast, [12] applies the FCS – MPC to the outer loop of a VSG – based ESS. Therein, the references of VSG active and reactive power are modified through the MPC so as it improves the frequency and voltage oscillations following load changes. The framework of [13] enables the ESS operator to provide frequency support while considering physical limits and lifetime of the employed energy storage. In this method, the frequency deviation and the RoCoF are first estimated by moving horizon estimation. These estimates are then used for an online – optimized FCS – MPC to compute the control actions. Refs. [14] and [15] apply the FCS – MPC to the control structure of islanded microgrids with multi – parallel VSCs. Akin to the conventional linear control, the droop loop generates the optimal voltage reference; however, the voltage tracking is realized by a FCS – MPC solution, resulting in improved transient performance. Model predictive power and voltage controls (MPPC & MPVC) are employed in [16] for a solar energy – based microgrid. The MPPC controls a buck – boost converter fed by a battery – type ESS, which smooths the fluctuating power from the solar generator. The employed inverters are then governed by incorporating the droop loop and the MPVC to ensure stable output voltages and appropriate power sharing.

The foregoing MPC approaches actualize short prediction horizons (up to 3), yielding still a poor dynamic performance in the converter current and voltage. Moreover, the closed – loop MPC system is not necessarily stable with short prediction and control horizons [17]. Ref. [18] derives properties of a reference tracking MPC scheme for general reference trajectories and non – linear discrete – time systems, wherein it is shown that large prediction horizon enhances stabilizability of reference tracking. On the other hand, one of the key difficulties facing future microgrids is the insufficient inertia owing to the rising shares of power electronic – based generators and concurrent decommissioning of SGs. Notwithstanding achievements in converter controls, few of them, e.g., [19] and [20], address the question *where* to place synthetic inertia devices in grids aimed at increasing the system resiliency and efficiency. Thus, *optimizing inertia placement* problem is the research gap which necessitates further emphasis and study.

1.2. Paper Contribution and Organization

Herein, we propose an enhanced discrete – time MPC – based reference tracker, superseding the inner – loop cascaded linear control of grid – forming converters. Our approach enjoys very simple parameter – tuning process and realizes large prediction horizons to achieve desired performance. Laguerre networks are used in the design framework to dramatically reduce computational burden [21]. Three control objectives (i.e., tracking reference trajectory, consideration given to the computational load, and flexible overcurrent protection) are integrated into a cost function whereby the optimal LF – DMPC system offers very short rise time, slight over – shoot, and robust control. Also, the swing – based and the reactive power droop controllers unify the reference generator aimed at inertia emulation and power sharing.

The rest of paper is presented as: Section II elucidates the conventional primary control of ac microgrids. Section III proposes the inner – loop LF – DMPC, wherein its design framework and cost function are detailed. In Section IV, describing function model of the proposed approach is derived and compared to the hierarchical linear controller from the stability point of view. The merits of proposed approach are verified by comparisons with droop and VSG controls in Section V. Finally, Section VI provides the conclusions.

2. Conventional Ac Microgrid Control

In this paper, the analyze and control of the VSC is executed in synchronously – rotating reference frame, where the quantities are shown in complex – valued space vectors marked with boldface letters.

Also, the set points and control commands are marked with "★" in superscripts. Fig. 1 depicts a grid – forming converter connected to the PoI by an LCL filter. The control system comprises two main loops, 1) outer – loop droop or VSG control, and 2) inner – loop cascaded voltage and current control. Each one is concisely explained here; readers are referred to [7] and [22] for further details.

2.1. Outer – Loop Control (Reference Generator)

Proper power sharing of converters in islanded ac microgrid is realized by the outer loop. Either droop control or VSG control forms voltage and frequency references for the inner loop. Superior to droop type, the VSG method can emulate inertia characteristic of real SGs. The equations describing droop and VSG controls are, respectively [7,22]:

$$\begin{cases} \omega_g = \omega_n - m_p\left(p_g - p_g^\star\right) \\ \left|u\right| = u_{fN} - m_q\left(q_g - q_g^\star\right) \end{cases} \tag{1}$$

and,

$$\begin{cases} \dot{\omega}_g = \dfrac{1}{J\omega_n}\left[p_g^\star - m_p\left(\omega_g - \omega_n\right) - p_g - D\left(\omega_g - \omega_n\right)\right] \\ \left|u\right| = u_{fN} - m_q\left(q_g - q_g^\star\right) \end{cases} \tag{2}$$

where all the parameters and variables are defined in Nomenclature. Remarkably, the angle of coordinate transforms (i.e., $abc \rightleftharpoons dq$) is obtained by:

$$\vartheta_g = \int \omega_g dt. \tag{3}$$

As per (1) or (2), the capacitor voltage reference in natural frame is:

$$\begin{cases} u_a = \left|u\right|\cos\left(\vartheta_g\right) \\ u_b = \left|u\right|\cos\left(\vartheta_g - \dfrac{2\pi}{3}\right) \\ u_c = \left|u\right|\cos\left(\vartheta_g - \dfrac{4\pi}{3}\right) \end{cases} \tag{4}$$

and, equal to:

$$\begin{aligned} \boldsymbol{u} &= \frac{2}{3}e^{-j\vartheta_g}\left(u_a + u_b e^{j\frac{2\pi}{3}} + u_c e^{j\frac{4\pi}{3}}\right) = \\ &\frac{2}{3}\left[\left(u_a - \frac{1}{2}u_b - \frac{1}{2}u_c\right)\cos\left(\vartheta_g\right) + \frac{\sqrt{3}}{2}\left(u_b - u_c\right)\sin\left(\vartheta_g\right)\right] + \\ &j\frac{2}{3}\left[\frac{\sqrt{3}}{2}\left(u_b - u_c\right)\cos\left(\vartheta_g\right) - \left(u_a - \frac{1}{2}u_b - \frac{1}{2}u_c\right)\sin\left(\vartheta_g\right)\right] \end{aligned} \tag{5}$$

in the dq – coordinate.

In a microgrid with multiple converters connected to the common ac bus through different line impedance, virtual impedance concept is applied; which yields improving power sharing accuracy [11]. Thus, the capacitor voltage reference is modified as:

$$\boldsymbol{u}_f^\star = \boldsymbol{u} - \underbrace{\left(R_{vi} + j\omega_g L_{vi}\right)}_{Z_{vi}} \boldsymbol{i}_g. \tag{6}$$

2.2. Inner – Loop Cascaded Linear Control (Reference Tracker)

Cascaded voltage and current controllers aim at desired tracking of (6). First, the standard proportional – integral (PI) voltage controller with current feedforward and cancellation of the dq – cross coupling forms the converter current reference as:

$$\boldsymbol{i}_c^\star = k_{pu}\left(\boldsymbol{u}_f^\star - \boldsymbol{u}_f\right) + k_{iu}\int\left(\boldsymbol{u}_f^\star - \boldsymbol{u}_f\right)dt + j\omega_g C_f \boldsymbol{u}_f + r_i \boldsymbol{i}_g. \tag{7}$$

The converter is then controlled by $\boldsymbol{u}_c^\star$ so that the converter tracks its current reference in (7).

$$\boldsymbol{u}_c^\star = k_{pi}\left(\boldsymbol{i}_c^\star - \boldsymbol{i}_c\right) + k_{ii}\int\left(\boldsymbol{i}_c^\star - \boldsymbol{i}_c\right)dt + j\omega_g L_{fc}\boldsymbol{i}_c + \boldsymbol{u}_f. \tag{8}$$

In general, the inner – loop cascaded linear control achieves limited bandwidth. This is due to the dynamical coupling of the control loops in the aforementioned cascaded controller [23]. On the contrary, single – loop voltage controllers can typically realize higher bandwidth compared to the cascaded controllers; however, they pose a challenge to converter current limiting in the case of faults or overloading [24]. To overcome this issue, we propose a fast inner – loop controller with the enhanced dynamic response and the inherent overcurrent protection capability.

3. Proposed Inner – Loop Controller

Discrete – time predictive control with Laguerre functions is used as the core of control system in Fig. 2. The design is based on optimizing the future control trajectory; i.e., the difference of control signal $\Delta\mathbf{u}(k) = \mathbf{u}(k) - \mathbf{u}(k-1)$. Presume the control horizon is finite. Then, $\Delta\mathbf{u}(k)\ \forall\ k = 0, 1, 2, \ldots, N_c - 1$ is attained with the proposed control rule, and the rest of $\Delta\mathbf{u}(k)\ \forall\ k = N_c, N_c + 1, \ldots, N_p$ is supposed to be zero.

Consider the state variable vector $\mathbf{x_m} = [\boldsymbol{i_c}\ \boldsymbol{u_f}\ \boldsymbol{i_g}]^T$. The discretized model of the plant (here, the LCL filter) is obtained as the first step (see Appendix A). Next, the augmented plant model to be utilized in the controller design is established as:

$$\underbrace{\begin{bmatrix} \Delta\mathbf{x_m}(k+1) \\ \mathbf{y}(k+1) \end{bmatrix}}_{\mathbf{x}(k+1)} = \underbrace{\begin{bmatrix} \mathbf{A_m} & 0_{3\times1} \\ \mathbf{C_m A_m} & 1 \end{bmatrix}}_{\mathbf{A}} \underbrace{\begin{bmatrix} \Delta\mathbf{x_m}(k) \\ \mathbf{y}(k) \end{bmatrix}}_{\mathbf{x}(k)} + \underbrace{\begin{bmatrix} \mathbf{B_m} \\ \mathbf{C_m B_m} \end{bmatrix}}_{\mathbf{B}} \Delta\mathbf{u}(k)$$

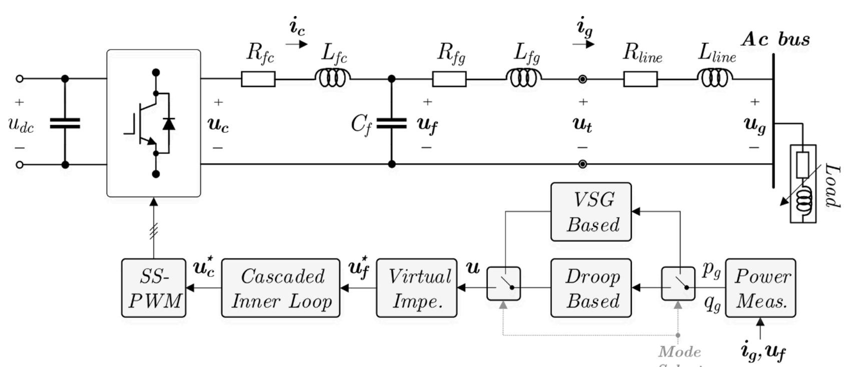

Fig. 1. Conventional droop/VSG control of an ac microgrid in dq – coordinate.

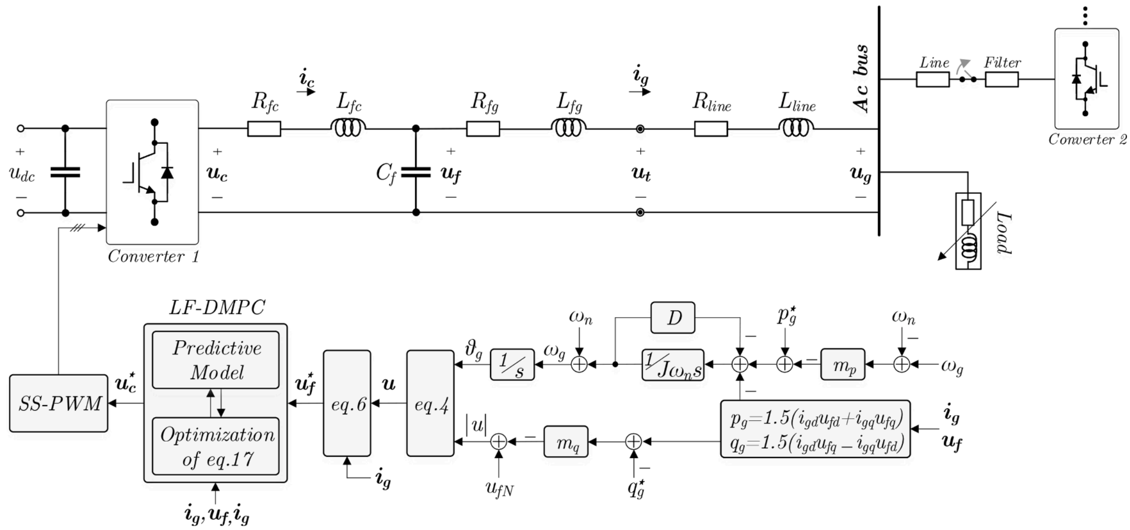

Fig. 2. Converter and its control scheme in $dq-$ coordinate.

$$\mathbf{y}(k)=\underbrace{\begin{bmatrix}0_{1\times3} & 1\end{bmatrix}}_{\mathbf{C}}\begin{bmatrix}\Delta\mathbf{x_m}(k)\\ \mathbf{y}(k)\end{bmatrix} \tag{9}$$

where $\Delta\mathbf{x_m}(k+1)=\mathbf{x_m}(k+1)-\mathbf{x_m}(k)$, and $\Delta\mathbf{x_m}(k)=\mathbf{x_m}(k)-\mathbf{x_m}(k-1)$. The corresponding matrices are defined in Appendix A.

Remark 1. the second row of the input matrix $\mathbf{u}=[\boldsymbol{u_c}\ \boldsymbol{u_t}]^T$ in the plant model must hold the PoI voltage reference. Albeit two inputs $\boldsymbol{u_c}$ and $\boldsymbol{u_t}$ enters the plant, but the converter voltage is only controllable, and $\Delta\boldsymbol{u_t}=0$.

3.1. Design Framework

Let k_i to be the current sampling time. The control signal trajectory $\Delta\boldsymbol{u_c}(k_i)$, $\Delta\boldsymbol{u_c}(k_i+1)$,..., $\Delta\boldsymbol{u_c}(k_i+k)$,..., is regarded as the impulse response of a stable dynamic system. Hence, a set of Laguerre functions denoted by $l_1^c(k)$, $l_2^c(k)$,..., $l_N^c(k)$ are employed to catch this dynamic response [21]. At an arbitrary future sampling instant k, the control signal is:

$$\Delta\boldsymbol{u_c}(k_i+k)=\mathbf{L_c}(k)^T\boldsymbol{\eta_c} \tag{10}$$

where the parameter vector $\boldsymbol{\eta_c}$ includes N Laguerre coefficients:

$$\boldsymbol{\eta_c}=[c_1\ c_2\ ...\ c_N]^T \tag{11}$$

and the vector form of the Laguerre function is:

$$\mathbf{L_c}(k+1)=\mathbf{A_l^c}\mathbf{L_c}(k) \tag{12}$$

with $\mathbf{L_c}(k)=[l_1^c(k)\ l_2^c(k)\ ...\ l_N^c(k)]^T$ and the initial condition of $\mathbf{L_c}(0)=[1\ -\alpha\ \alpha^2\ ...\ (-\alpha)^{N-1}]^T$.

Also, $\mathbf{A_l^c}$ is a $N\times N$ matrix and function of the parameters α and $\beta=(1-\alpha^2)$ as:

$$\mathbf{A_l^c}=\begin{bmatrix}\alpha & 0 & 0 & \cdots & 0\\ \beta & \alpha & 0 & & 0\\ -\alpha\beta & \beta & \alpha & & 0\\ \vdots & & & \ddots & 0\\ (-\alpha)^{N-2}\beta & (-\alpha)^{N-3}\beta & (-\alpha)^{N-4}\beta & & \alpha\end{bmatrix}. \tag{13}$$

Using Laguerre functions, the augmented plant model (i.e., $\mathbf{A},\mathbf{B},\mathbf{C}$) with the initial state variable vector $\mathbf{x}(k_i)$ and the control signal (10), the prediction of future state variable vector, i.e., $\mathbf{x}(k_i+k)$, and the plant output $\mathbf{y}(k_i+k)$ at arbitrary sampling time of k are written, respectively as:

$$\mathbf{x}(k_i+k)=\mathbf{A}^k\mathbf{x}(k_i)+\sum_{j=0}^{k-1}\mathbf{A}^{k-j-1}\mathbf{B_1}\mathbf{L_c}(j)^T\boldsymbol{\eta_c} \tag{14}$$

$$\mathbf{y}(k_i+k)=\mathbf{C}\mathbf{A}^k\mathbf{x}(k_i)+\sum_{j=0}^{k-1}\mathbf{C}\mathbf{A}^{k-j-1}\mathbf{B_1}\mathbf{L_c}(j)^T\boldsymbol{\eta_c} \tag{15}$$

with $\mathbf{B_1}$ being the first column of $\mathbf{B}$, just correspond to the input $\boldsymbol{u_c}$.

As per formulations above, the prediction of state variable vector and output variable are obtained based on the coefficient vector $\boldsymbol{\eta_c}$, instead of $\Delta\mathbf{u}$. Next, $\boldsymbol{\eta_c}$ is optimized and computed in the controller design.

3.2. Multiobjective Cost Function

The cost function J actualizes three control objectives: 1) minimizing the error between the prediction of capacitor voltage ($\boldsymbol{u_f}$) and its set point ($\boldsymbol{u_f^\star}\rightarrow$ coming from reference generator), 2) consideration given to the size of $\boldsymbol{\eta_c}$, and 3) flexible overcurrent protection capability of the converter in the case of faults or overloading. Each term has a weighting matrix ($\mathbf{Q}$, $\mathbf{R_L}$, and $\boldsymbol{\Lambda}$, respectively), and assigning a larger value to the weight of interest yields convergence of the cost function toward that specific goal. If we want the control signal to move cautiously, then high value is selected for $\mathbf{R_L}$. Accordingly, it takes longer for the control signal to reach its steady state [i.e., the values in $\Delta\mathbf{u}$, cf. (10), reduce more slowly compared to the case with e.g., $\mathbf{R_L}$ set to $\mathbf{0}_{N\times N}$]. Thus, larger control horizon should be considered as the optimal control energy is distributed over a longer period of future time. In contrast, $\Delta\mathbf{u}$ can move more freely with lower $\mathbf{R_L}$ and shorter control horizon is required.

In order to incorporate the set point signal into J, the state variable vector $\mathbf{x}(k_i+k)$ needs to be re-defined as:

$$\mathbf{x}(k_i+k)=\left[\Delta\mathbf{x_m}(k_i+k)^T\ \mathbf{y}(k_i+k)-\boldsymbol{u_f^\star}(k_i)\right]^T. \tag{16}$$

Hence, the cost function is formulated as:

$$J=\sum_{k=1}^{N_p}\mathbf{x}(k_i+k)^T\mathbf{Q}\mathbf{x}(k_i+k)+\boldsymbol{\eta_c}^T\mathbf{R_L}\boldsymbol{\eta_c}+\mathbf{x}(k_i+k)^T\boldsymbol{\Lambda}\mathbf{x}(k_i+k) \tag{17}$$

with $\mathbf{Q}=\mathbf{C}^T\mathbf{C}$, and $\mathbf{R_L}$ ($N\times N$) is a diagonal matrix with weight factor of $r_w\geq0$ on its main diagonal. Also, $\boldsymbol{\Lambda}$ is:

$$\mathbf{\Lambda} = \begin{bmatrix} \lambda & 0 & 0 & 0 \\ 0 & 0 & 0 & 0 \\ 0 & 0 & 0 & 0 \\ 0 & 0 & 0 & 0 \end{bmatrix} \tag{18}$$

where,

$$\lambda = \begin{cases} 0 & \text{if} \left| \boldsymbol{i_c}(k_i) \right| \le I_{c,max} \\ \infty & \text{if} \left| \boldsymbol{i_c}(k_i) \right| > I_{c,max} \end{cases}. \tag{19}$$

It is noteworthy that λ associates with the first element in (16), i.e., $\boldsymbol{i_c}$, which takes ∞ if the sensed converter – side current is higher than $I_{c,max}$. Accordingly, the controller curbs the current to $I_{c,max}$, and ignores the other objectives in (17).

3.3. Minimization of the Objective Function

Defining convolution sum as:

$$\boldsymbol{\varphi}(k)^T = \sum_{j=0}^{k-1} \mathbf{A}^{k-j-1}\mathbf{B_1}\mathbf{L_c}(j)^T \tag{20}$$

the equation (14) becomes:

$$\mathbf{x}(k_i+k) = \mathbf{A}^k\mathbf{x}(k_i) + \boldsymbol{\varphi}(k)^T\boldsymbol{\eta_c}. \tag{21}$$

Substituting (21) into the cost function formulation (17) yields:

$$J = \boldsymbol{\eta_c}^T\left[\sum_{k=1}^{N_p}\boldsymbol{\varphi}(k)(\mathbf{Q}+\mathbf{\Lambda})\boldsymbol{\varphi}(k)^T + \mathbf{R_L}\right]\boldsymbol{\eta_c} + 2\boldsymbol{\eta_c}^T\left[\sum_{k=1}^{N_p}\boldsymbol{\varphi}(k)(\mathbf{Q}+\mathbf{\Lambda})\mathbf{A}^k\right]\mathbf{x}(k_i) + \sum_{k=1}^{N_p}\mathbf{x}(k_i)^T\left(\mathbf{A}^T\right)^k(\mathbf{Q}+\mathbf{\Lambda})\mathbf{A}^k\mathbf{x}(k_i). \tag{22}$$

The partial derivative of (22) is then set to zero to find the optimal solution of the coefficient vector $\boldsymbol{\eta_c}$. Accordingly, $\boldsymbol{\eta_c}$ is obtained as:

$$\boldsymbol{\eta_c} = -\left[\sum_{k=1}^{N_p}\boldsymbol{\varphi}(k)(\mathbf{Q}+\mathbf{\Lambda})\boldsymbol{\varphi}(k)^T + \mathbf{R_L}\right]^{-1}\left[\sum_{k=1}^{N_p}\boldsymbol{\varphi}(k)(\mathbf{Q}+\mathbf{\Lambda})\mathbf{A}^k\right]\mathbf{x}(k_i). \tag{23}$$

Once achieving the optimal coefficient vector $\boldsymbol{\eta_c}$, the receding horizon control rule is formed as:

$$\Delta\boldsymbol{u_c}(k_i) = \mathbf{L_c}(0)^T\boldsymbol{\eta_c}. \tag{24}$$

In each sampling instant, the control signal is updated using (24), i.e., $\boldsymbol{u}_c^\star(k_i+1) = \boldsymbol{u}_c^\star(k_i) + \Delta\boldsymbol{u_c}(k_i)$, and enters the SS – PWM block to generate the firing pulses of the converter (cf. Fig. 2).

Remark 2. five controlling parameters, marked with numbers in the following, are selected properly considering a compromise between good dynamic performance and computational load; 1) α: defines the pole of the discrete – time Laguerre network and it must be within $0 \le \alpha < 1$ for stability of the network. With lower α, Laguerre functions decay to zero at faster speed (i.e., with fewer samples). 2) N: capturing the dynamics of the impulse response is improved as N increases (independent of the choice of α), however, it also enlarges the size of computational matrices. A compromise should be made between the approximation of the impulse response and the computational load. 3) N_p, and 4) N_c: large prediction horizon and control horizon are required to achieve desired performance. It is noteworthy that $N_p \ge N_c$. And 5) weight factor on the main diagonal of $\mathbf{R_L}$ ($r_w \ge 0$): is used as a tuning parameter for desired closed – loop performance. Lower r_w means we would not want to pay attention to the size of $\boldsymbol{\eta_c}$ and vice versa [cf. (17)].

Remark 3. the operator only determines the weighting matrix $\mathbf{R_L}$ (based on the required dynamic performance) in the cost function; And $\mathbf{Q}$ and $\mathbf{\Lambda}$ are selected as $\mathbf{C}^T\mathbf{C}$ and (18), respectively.

4. Stability Assessment

Describing function (DF) method [25] is applied to study frequency response of the proposed LF – DMPC. As per DF analysis, a non – linear element can be defined by a corresponding linear frequency response if a perturbation signal entered to the non – linear part excites a sinusoidal response at the same frequency [26]. To this end, the phase voltage reference (e.g., $u_{f,a}^\star$) is perturbed by a small sinusoidal voltage frequency sweep. Here, the disturbance amplitude A_p is considered 5 V and its frequency f_p varies from 50 Hz – 5 kHz. The closed – loop DF of the inner – loop LF – DMPC is then attained as:

$$DF\left(f_p\right) = \frac{A_m\left(f_p\right)}{A_p}\angle\vartheta_m\left(f_p\right) \tag{25}$$

where $A_m(f_p)$ and $\vartheta_m(f_p)$ are the measured capacitor phase voltage (i.e., $u_{f,a}$) amplitude and phase angle at each f_p, respectively. Next, a sixth – order transfer function approximates the measured DF (25) through " *tfest*" command in MATLAB, resulting in:

$$\mathrm{DF}(s) = \frac{-3.223e^{18}s + 4.355e^{20}}{s^6 + 847.2s^5 + 5.967e^7s^4 - 2.648e^{10}s^3 - 5.957e^{14}s^2 - 4.935e^{16}s - 5.036e^{19}}. \tag{26}$$

Moreover, the inner – loop transfer function using cascaded linear control is obtained as:

$$\mathrm{G_{CLC}}(s) = \frac{\mathrm{H_1H_2G_dG_iG_u}}{1 + \mathrm{H_1H_2} + \mathrm{H_1G_dG_i} + \mathrm{H_1H_2G_dG_iG_u}} \tag{27}$$

in which $\mathrm{H_1}(s)$ and $\mathrm{H_2}(s)$ are, respectively:

$$\mathrm{H_1}(s) = \frac{1}{R_{fc} + sL_{fc}} \tag{28}$$

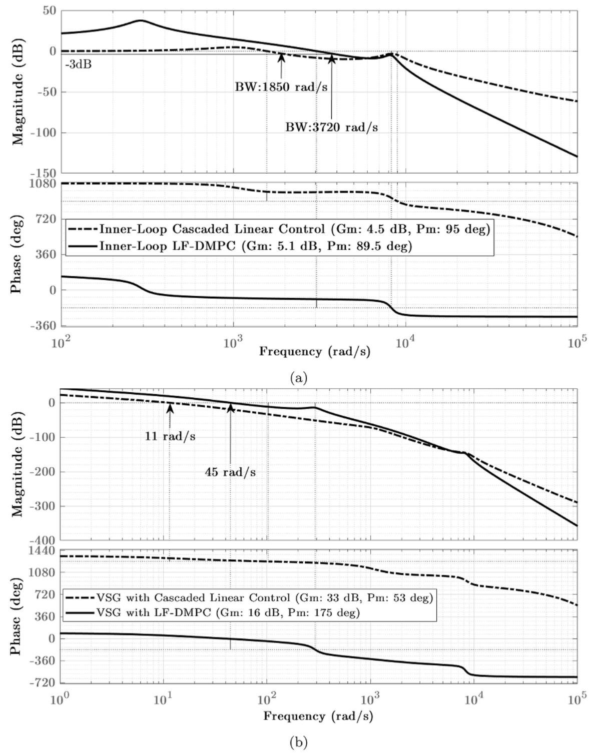

Fig. 3. Frequency response of the (a) inner – loop controller, and (b) VSG controller.

$$\mathrm{H_2(s)} = \frac{1}{sC_f} \tag{29}$$

and, the corresponding PI – voltage and current controllers are denoted with $\mathrm{G_u(s)}$ and $\mathrm{G_i(s)}$, respectively. Also, $\mathrm{G_d(s)} = e^{-T_s s}$ models the computational time and the PWM switching with T_s being the sampling period (it should be noted that the delay in LF – DMPC method is included in the MATLAB simulation model). Consequently, the VSG transfer function is derived as:

$$\mathrm{G(s)} = \begin{cases} \mathrm{G_S.DF.G_L} & \text{for LF} - \text{DMPC} \\ \mathrm{G_S.G_{CLC}.G_L} & \text{for cascaded linear control} \end{cases} \tag{30}$$

where:

$$\mathrm{G_S(s)} = \frac{1}{J\omega_n s + D}\cdot\frac{1}{s} \tag{31}$$

$$\mathrm{G_L(s)} = \frac{3u_{fN}}{2}\cdot\frac{a_1 s^2 + a_2 s + a_3}{(R^2 + X^2)\left[(R + sL)^2 + X^2\right]} \tag{32}$$

are the transfer function from power to electric potential angle, and the transfer function from output power to electric potential phase angle, respectively [11,27]. The corresponding parameters of (32) are defined in Appendix B.

The bode plot in Fig. 3(a) illustrates the frequency response of the inner – loop controllers. As observed from this figure, gain margin (Gm) and phase margin (Pm) stability indices are almost identical in both methods; however, the proposed inner – loop LF – DMPC enjoys about two times larger bandwidth. Hence, it results in a better dynamic performance compared to the cascaded linear control (see Section V). Fig. 3 (b) compares the overall VSG controllers in terms of stability indices. The gain and phase margins in the MPC – based VSG are 16 dB and 175 deg., respectively. These indices are 33 dB and 53 deg. in the case of cascaded linear controlled VSG.

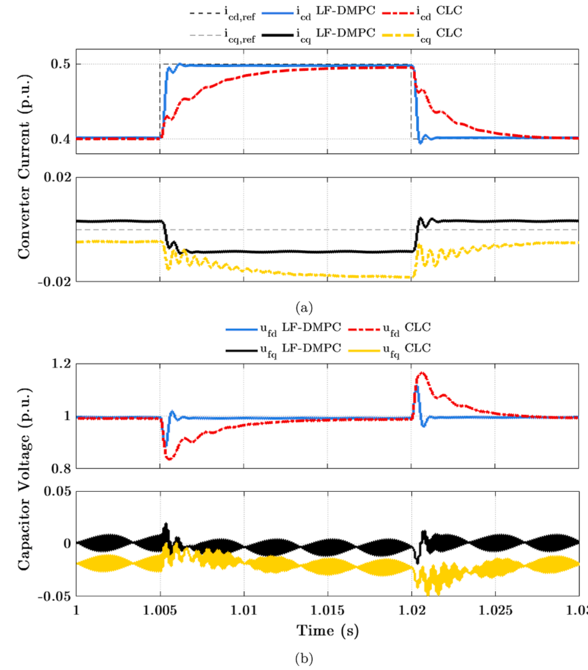

Fig. 4. Simulation validation of the proposed LF – DMPC based VSG under step changes in the microgrid load, (a) converter current, (b) capacitor voltage.

5. Simulation Results and Discussions

Detailed model simulation of a 2 – converter ac microgrid (see Fig. 2) is built in MATLAB Simulink R2021a update 4 to depict the efficacy of the proposed inner – loop LF – DMPC. The method is then compared with the cascaded linear control – based VSG. The specifications of the system under study are provided in Table I. Moreover, the system base values are selected according to the PoI voltage reference and the maximum load demand. The converters only control ac – side quantities (converter current and voltage), and the dc – link voltages are considered to be constant. The converters are connected to a variable load through LCL filters and transmission lines to emulate step – up and step – down changes in the local demand. In addition, a three – phase fault with a 0.136 Ω (0.0213 p.u.) ground resistance occurs on the common ac – bus (cf. Fig. 2) to illustrate the inherent overcurrent protection of the employed converters.

5.1. Dynamic and Static Performance

The dynamic response of the controllers is analyzed to show the properties of the proposed inner – loop LF – DMPC compared to the cascaded linear controller. Fig. 4(a) depicts the converter current response using LF – DMPC and cascaded linear controllers under step – up and step – down changes in the load (i.e., the demand is either 0.8 p.

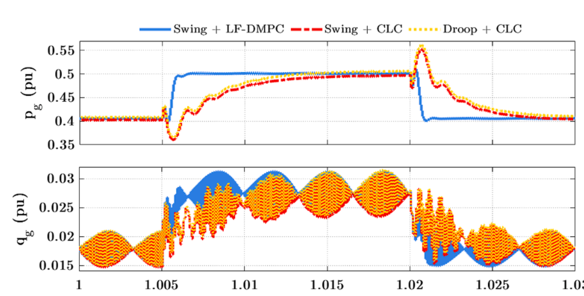

Fig. 5. Converter power under step changes in the microgrid load (remark 5: the load is supplied by two same converters).

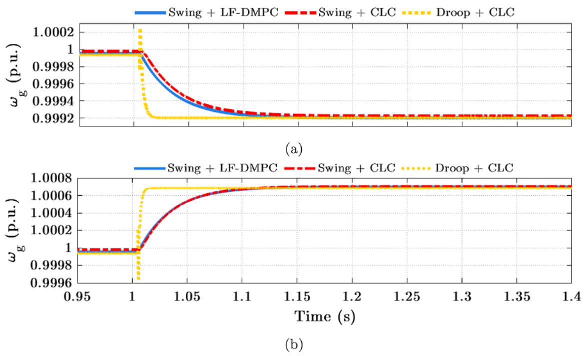

Fig. 6. Microgrid frequency following the (a) step – up, and (b) step – down load change occurred at $t = 1.005$ s.

u. or 1 p.u.). As observed, the proposed controller regulates the d – axis converter current without any overshoot to its new set point about 10 times faster than the linear controller. And, the q– axis converter current is controlled with less transient oscillations by the LF – DMPC. In addition, as per Fig. 4(b), the capacitor voltage fluctuations and settling time using the proposed approach are well improved compared to the cascaded linear controller (remarkably, the slight ripple with amplitude of 0.007 p.u. mounted on the q – axis voltage is caused by the converter switching process). Hence, better dynamic performance is realized in both d– and q– axes, owing to higher bandwidth of the inner – loop LF – DMPC without sacrificing the robustness. It is noteworthy that the outputs of one converter is only presented here. The results associated to the second converter are the same as Fig. 4 since we assumed the converters supply the load evenly.

The converter active power regulated by the controllers understudy is presented in Fig. 5. Clearly, the cascaded linear controller with droop– and swing – based outer loops yields almost the same transient response (rise time: 10 ms and overshoot: 0.05 p.u.). In contrast, these indices are dramatically enhanced to about 1.5 ms and 0 p.u., respectively by the proposed controller. Moreover, the comparison of reactive power responses in Fig. 5 demonstrates that the LF – DMPC method provides better dynamic performance. It is worth noting that the negligible ripple with amplitude of 0.006 p.u. in the output reactive power is caused by the converter switching process.

Fig. 6 illustrates the system frequency response following step – up and step – down load change (0.8 p.u. → 1 p.u. and 0.8 p.u. → 0.6 p.u.) scenarios. When the converter controller is augmented with the swing – based outer loop, the system frequency rate of change is improved by 15% compared with the case in which droop – based outer loop is applied. This signifies that the basic swing equation embedded in the converter controller can effectively enhance the frequency stability.

5.2. Overcurrent Protection

In this subsection, the overcurrent protection capability of the proposed controller under fault condition is examined. The fault behavior of the inner – loop LF – DMPC is flexibly designed by selecting the value of $|\boldsymbol{i}_c|$. Here, the overcurrent limit is chosen 1 p.u. as an example. The fault scenario is simulated with connecting the common ac – bus to the ground through a 0.136 Ω (0.0213 p.u.) resistance. A circuit breaker is used in the fault emulation scenario so as to disconnect the fault from the rest of microgrid after 10 ms. Fig. 7 presents the fault simulation results. At the beginning, the converter operates in 1 p.u. d – axis voltage with 0.8 p.u. load. Then, the fault occurs at 1.005 s. The behavior of the converter without overcurrent protection capability [i.e., (17) lacks the third term] is presented in Fig. 7(a). Undesirably, the d– and q– axis currents exceed the permissible limit following the fault instant as the converter strives to maintain the capacitor voltage at its nominal value. Considering the overcurrent protection term in (17) effectively limits the converter current amplitude. As observed from Fig. 7(b), the current and voltage in the SRF reach their new set points within very short transient times (1.5 ms) with slight overshoots. After 10 ms from the fault occurrence, the fault is cleared from the ac – bus by the employed circuit breaker. This allows the inner – loop LF – DMPC to retrieve its prefault operation and end the current limiting.

5.3. Parameter – tuning Sensitivity

The proposed reference tracking MPC scheme offers a very simple parameter – tuning process, which makes the method appealing for practical applications. Fig. 8 depicts the impact of each controlling parameter on the converter performance (in each scenario, the rest of parameters are considered as the benchmark in Table 1). The dynamic response of the converter in terms of different α is illustrated in Fig. 8(a). With lower α, Laguerre functions decay to zero at faster speed. Accordingly, the controlled quantities reach their new set point faster. Fig. 8(b) pictures the impact of different N on the operation of the converter. More accurate response is obtained using higher N. The operator should select N considering a compromise between the approximation of the impulse response and the computational load (e.g., herein, N set to 4 or 8 yields almost the same results; hence, 4 is preferred owing to less computational burden). Also, desired performance is realized using large prediction horizons. For example, as observed from Fig. 8(c), increasing the prediction horizon yields much better transients in the converter current and voltage, i.e., slighter overshoot and shorter settling time. Finally, the performance of the converter in terms of different r_w is depicted in Fig. 8(d). Indeed, shorter rise time, but, slightly oscillatory response is obtained with higher r_w. The operator can select r_w considering the desired closed – loop performance (we recommend r_w to be between 0.1 and 1).

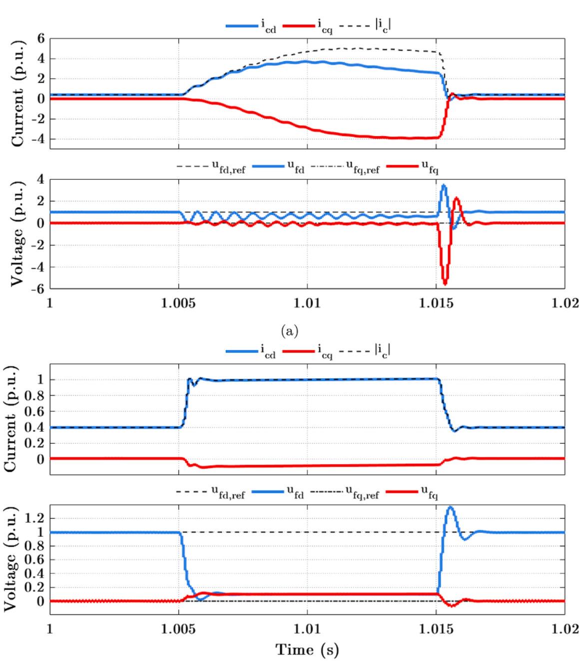

Fig. 7. Fault scenario simulations, (a) without current limiter, (b) with current limiter (remark 6: to model the load fault, a small resistance is paralleled with the microgrid load).

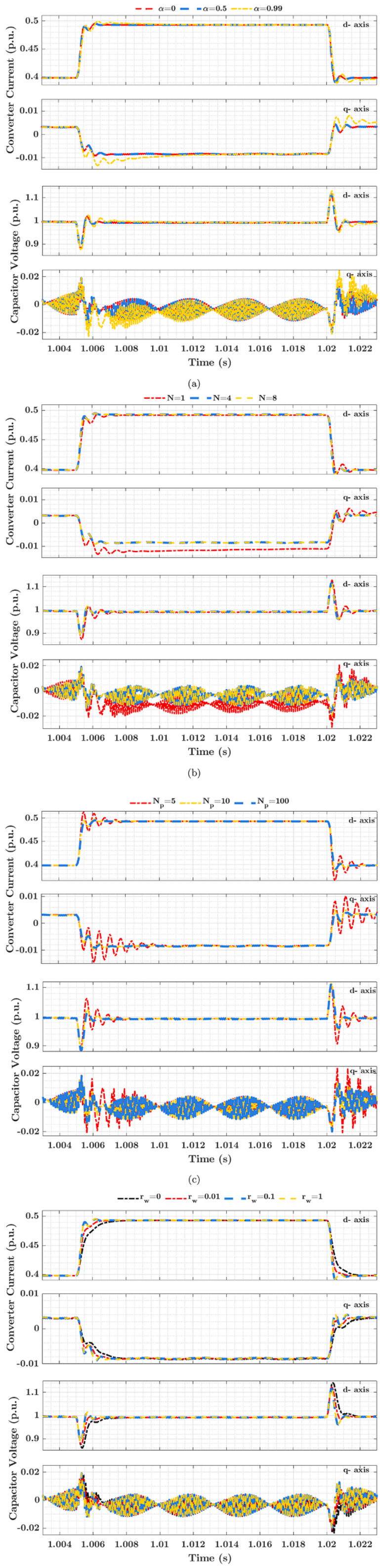

Fig. 8. Converter performance with different (a) α, (b) N, (c) N_p, and (d) r_w.

Table 1
Parameters of the System

	Parameter	Value	Parameter	Value
Grid – Converter	u_{fN}	$\sqrt{2/3}.400$ V	C_f	10 μF
	ω_n, f_{sw}	$2\pi.50$ rad/s, 8 kHz	u_{dc}	750 V
	L_{fc}, L_{fg}, L_{line}	2.94, 1.96, 0.3 mH	p_{load}	15←20→25 kW
	R_{fc}, R_{fg}, R_{line}	0.1, 0.1, 0.23 Ω	$p_g\bigstar, q_g\bigstar$	10 kW, 0 kVAr
Control	α	[0.5 0.5]	J	1 kg.m^2
	N	[6 6]	D	5000
	N_p	100	m_p, m_q	$9.4e^{-5}, 1.3e^{-3}$
	N_c	10	k_{pi}, k_{ii}	14.7781, $7.4283e^4$
	r_w	0.1	k_{pu}, k_{iu}	0.0251,63.1655
	λ	0 or ∞	Z_{vi}	$0.3 + j0.0314$

Remark 4: the parameters of the two converters are assumed to be identical.

6. Conclusions

This paper proposed a multiobjective Laguerre functions – based discrete – time model predictive control, superseding the inner – loop cascaded linear controller of conventional grid – forming converters. The proposed method allows using large prediction horizons and very fast dynamic response without sacrificing the control robustness. Laguerre networks were used in the design framework to dramatically reduce computational burden. Moreover, the inherent overcurrent protection capability of the method limits the converter current to a preset value in the case of faults or converter overloading. Also, the outer – loop was formed by the swing – based and the reactive power droop controllers aimed at inertia emulation and proper power sharing. The dynamic response of the proposed approach was compared with the cascaded linear control to highlight its merits. The properties of the method were validated by detailed model simulations in MATLAB. As a future work, the number of required sensors in such system can be reduced using observer – based solutions. One may find the implementation of the controller complicated in large scale systems compared to the conventional hierarchical linear control, which can be seen as the downside of our method; however, we emphasize that the parameter – tuning process is very simple and effective.

Credit Author Statement

Meysam Saeedian and Edris Pouresmaeil worked on conceptualization, methodology, simulation, validation, formal analysis, writing original draft preparation, writingreview and editing.

Edris Pouresmaeil and Oriol Gomis-Bellmunt did the final review and editing.

All authors have read and agreed to the published version of the manuscript.

Declaration of Competing Interest

We wish to confirm that there are no known conflicts of interest associated with this publication and there has been no significant financial support for this work that could have influenced its outcome. We confirm that the manuscript has been read and approved by all named authors and that there are no other persons who satisfied the criteria for authorship but are not listed. We further confirm that the order of authors listed in the manuscript has been approved by all of us. We confirm that we have given due consideration to the protection of intellectual property associated with this work and that there are no impediments to publication, including the timing of publication, with respect to intellectual property. In so doing we confirm that we have followed the regulations of our institutions concerning intellectual property. We understand that the Corresponding Author is the sole contact for the Editorial process (including Editorial Manager and direct communications with the office). He/she is responsible for communicating with the other authors about progress, submissions of revisions and final approval of proofs. We confirm that we have provided a current, correct email address which is accessible by the Corresponding Author.

Appendix A. Discrete − Time Model of the LCL Filter

The continuous − time plant model in the synchronous coordinate is defined by:

$$\frac{d}{dt}\underbrace{\begin{bmatrix} i_c \\ u_f \\ i_g \end{bmatrix}}_{\mathbf{x_m}} = \underbrace{\begin{bmatrix} -j\omega_n + \frac{R_{fc}}{L_{fc}} & -\frac{1}{L_{fc}} & 0 \\ \frac{1}{C_f} & -j\omega_n & -\frac{1}{C_f} \\ 0 & \frac{1}{L_{fg}} & -j\omega_n + \frac{R_{fg}}{L_{fg}} \end{bmatrix}}_{\mathbf{A_c}} \underbrace{\begin{bmatrix} i_c \\ u_f \\ i_g \end{bmatrix}}_{\mathbf{x_m}} + \underbrace{\begin{bmatrix} \frac{1}{L_{fc}} & 0 \\ 0 & 0 \\ 0 & -\frac{1}{L_{fg}} \end{bmatrix}}_{\mathbf{B_c}} \underbrace{\begin{bmatrix} u_c \\ u_t \end{bmatrix}}_{\mathbf{u}}$$

$$\mathbf{y} = \underbrace{\begin{bmatrix} 0 & 1 & 0 \end{bmatrix}}_{\mathbf{C_c}} \underbrace{\begin{bmatrix} i_c \\ u_f \\ i_g \end{bmatrix}}_{\mathbf{x_m}}. \tag{33}$$

The model is then discretized using the MATLAB function "$c2dm$" with the specified sampling interval $T_s = \frac{1}{2f_{sw}}$; $[\mathbf{A_m}, \mathbf{B_m}, \mathbf{C_m}, \mathbf{D_m}] = c2dm(\mathbf{A_c}, \mathbf{B_c}, \mathbf{C_c}, \mathbf{D_c}, T_s, 'zoh')$. Sampling of the state variable vector is supposed to be synchronized with the SS − PWM.

B. Parameters of the Transfer Function $G_L(s)$

The parameters corresponding to (32) are defined as [27]:

$$a_1 = u_{gN} L L_{line} \left[R\sin(\vartheta_{g0}) + X\cos(\vartheta_{g0})\right] - u_{fN} L X L_{line} \tag{34}$$

$$\begin{aligned} a_2 = 2u_{gN} L R_{line} \left[R\sin(\vartheta_{g0}) + X\cos(\vartheta_{g0})\right] + 2u_{fN} L_{vi} X \sin(\vartheta_{g0}) \left[R\sin(\vartheta_{g0}) - X\cos(\vartheta_{g0})\right] \\ -2u_{fN} L X R_{line} - u_{gN} L_{vi} \sin(\vartheta_{g0}) \left(R^2 - X^2\right) \end{aligned} \tag{35}$$

$$\begin{aligned} a_3 = u_{gN}\left(R^2 + X^2\right)\left[R\sin(\vartheta_{g0}) + X\cos(\vartheta_{g0})\right] + 2u_{fN} R_{vi} X \sin(\vartheta_{g0}) \left[R\sin(\vartheta_{g0}) - X\cos(\vartheta_{g0})\right] \\ -2u_{gN} R_{vi} R^2 \sin(\vartheta_{g0}) \end{aligned} \tag{36}$$

where $R = R_{vi} + R_{line}$, $L = L_{vi} + L_{line}$, and $X = \omega_n L$.

References

[1] R.H. Lasseter, Microgrids, IEEE Power Engineering Society Winter Meeting 1 (2002) 305–308.

[2] R. Mourouvin, J.C. Gonzalez-Torres, J. Dai, et al., Understanding the role of VSC control strategies in the limits of power electronics integration in AC grids using modal analysis, Electric Power Systems Research 192 (2021) 106930, https://doi.org/10.1016/j.epsr.2020.106930.

[3] M. Saeedian, R. Sangrody, M. Shahparasti, et al., Grid-following DVI-based converter operating in weak grids for enhancing frequency stability, IEEE Trans. Power Delivery 37 (1) (2022) 338–348.

[4] L. Harnefors, J. Kukkola, M. Routimo, et al., A universal controller for grid-connected voltage-source converters, IEEE Journal of Emerg. and Selec. Topics in Power Electron. 9 (5) (2021) 5761–5770.

[5] F. Blaabjerg, R. Teodorescu, M. Liserre, A.V. Timbus, Overview of control and grid synchronization for distributed power generation systems, IEEE Trans. Ind. Electron. 53 (5) (2006) 1398–1409.

[6] Z. Li, et al., Virtual synchronous generator and SMC based cascaded control for voltage-source grid-supporting inverters, IEEE Journal of Emerg. and Selec. Topics in Power Electron.10.1109/JESTPE.2021.3056576.

[7] S. D'Arco, J.A. Suul, O.B. Fosso, Automatic tuning of cascaded controllers for power converters using eigenvalue parametric sensitivities, IEEE Trans. Ind. Appl. 51 (2) (2015) 1743–1753.

[8] A. Rafiee, Y. Batmani, F. Ahmadi, H. Bevrani, Robust load-frequency control in islanded microgrids: Virtual synchronous generator concept and quantitative feedback theory, IEEE Trans. Power Systems 36 (6) (2021) 5408–5416.

[9] A. Hussain, S. Hasan, S. Patil, W. Shireen, Fast frequency regulation in islanded microgrid with SGs using model-based load estimation, IEEE Trans. Energy Conversion 36 (4) (2021) 3188–3198.

[10] M. Pourmohammad, M. Toulabi, A.M. Ranjbar, Application of state feedback controller to ensure robust d-stable operation of virtual synchronous generators, IEEE Trans. Energy Conversion 36 (2) (2021) 602–610.

[11] C. Zheng, T. Dragicevic, F. Blaabjerg, Model predictive control-based virtual inertia emulator for an islanded alternating current microgrid, IEEE Trans. Ind. Electron. 68 (8) (2021) 7167–7177.

[12] B. Long, Y. Liao, K.T. Chong, et al., MPC-controlled virtual synchronous generator to enhance frequency and voltage dynamic performance in islanded microgrids, IEEE Trans. Smart Grid 12 (2) (2021) 953–964.

[13] U. Tamrakar, D.A. Copp, T. Nguyen, et al., Optimization-based fast-frequency estimation and control of low-inertia microgrids, IEEE Trans. Energy Conversion 36 (2) (2021) 1459–1468.

[14] T. Chen, O. Abdel-Rahim, F. Peng, H. Wang, An improved finite control set-MPC-based power sharing control strategy for islanded AC microgrids, IEEE Access 8 (2020) 52676–52686.

[15] Y. Li, Z. Zhang, C. Hu, M. Abdelrahem, et al., A full state-variable direct predictive control for islanded microgrids with parallel converters, IEEE Journal of Emerg. and Selec. Topics in Power Electron. 9 (4) (2021) 4615–4628.

[16] Y. Shan, J. Hu, Z. Li, J.M. Guerrero, A model predictive control for renewable energy based AC microgrids without any PID regulators, IEEE Trans. Power Electron. 33 (11) (2018) 9122–9126.

[17] L. Grüne, J. Pannek, Nonlinear Model Predictive Control: Theory and Algorithms, Springer-Verlag London, 1st ed., New York, NY, USA, 2011.http://www.springer.com/978-0-85729-500-2

[18] J. Köhler, M.A. Müller, F. Allgöwer, Nonlinear reference tracking: An economic model predictive control perspective, IEEE Trans. Automatic Control 64 (1) (2019) 254–269.
[19] B.K. Poolla, D. Groß, F. Dörfler, Placement and implementation of grid-forming and grid-following virtual inertia and fast frequency response, IEEE Trans. Power Systems 34 (4) (2019) 3035–3046.
[20] B.K. Poolla, S. Bolognani, F. Dörfler, Optimal placement of virtual inertia in power grids, IEEE Trans. Automatic Control 62 (12) (2017) 6209–6220.
[21] L. Wang, Model Predictive Control System Design and Implementation Using MATLAB, Springer, London, 2009.First edition
[22] A. Bidram, A. Davoudi, Hierarchical structure of microgrids control system, IEEE Trans. Smart Grid 3 (4) (2012) 1963–1976.
[23] V. Pirsto, J. Kukkola, M. Hinkkanen, Multifunctional cascade control of voltage-source converters equipped with an LC filter, IEEE Trans. Ind. Electron. 69 (3) (2022) 2610–2620.
[24] H. Kim, H. Jung, S. Sul, Discrete-time voltage controller for voltage source converters with LC filter based on state-space models, IEEE Trans. Ind. Appl. 55 (1) (2019) 529–540.
[25] A. Gelb, W. Velde, Multiple-Input Describing Functions and Nonlinear System Design, McGraw-Hill, New York, USA, 1968.First edition
[26] R. Heydari, T. Dragicevic, F. Blaabjerg, High-bandwidth secondary voltage and frequency control of VSC-based AC microgrid, IEEE Trans. Power Electron. 34 (11) (2019) 11320–11331.
[27] J. Chen, T. O'Donnell, Parameter constraints for virtual synchronous generator considering stability, IEEE Trans. Power Systems 34 (3) (2019) 2479–2481.